

Properties of the ${}^7\text{He}$ ground state studied by the ${}^6\text{He}(d,p){}^7\text{He}$ reaction

A. A. Bezbakh , M. S. Golovkov , A. S. Denikin , R. Wolski ,
S. G. Belogurov , D. Biare*, V. Chudoba , A. S. Fomichev*,
E. M. Gazeeva , A. V. Gorshkov , G. Kaminski , B. R. Khamidullin ,
M. Khirk , S. A. Krupko , B. Mauyey , I. A. Muzalevskii*,
A. M. Quynh , S. I. Sidorchuk**, R. S. Slepnev*, A. Swiercz ,
G. M. Ter-Akopian  and B. Zalewski*

*Flerov Laboratory of Nuclear Reactions, JINR,
Dubna 141980, Russia

[†]Nuclear Physics Department, Dubna State University,
Dubna 141982, Russia

[‡]National Research Nuclear University MEPhI,
Moscow 115409, Russia

[§]Institute of Physics, Silesian University in Opava,
Opava 74601, Czech Republic

[¶]Heavy Ion Laboratory, University of Warsaw,
Warsaw 02-093, Poland

^{||}Department of Nuclear-Physical Materials Science,
Kazan Federal University, Kazan 420111, Russia

^{**}Skobeltsyn Institute of Nuclear Physics,
Moscow State University, Moscow 119991, Russia

^{††}L.N. Gumilyov Eurasian National University,
Astana 010008, Kazakhstan

^{‡‡}Nuclear Research Institute,
Dalat 670000, Vietnam

^{§§}Department of Nuclear Physics,
Voronezh State University, 1 Universitetskaya pl.,
Voronezh 394018, Russia
bezbakh@jinr.ru

Received 20 September 2023

Revised 14 December 2023

Accepted 18 December 2023

Published 3 February 2024

The ${}^7\text{He}$ nucleus was studied using the ${}^6\text{He}(d,p){}^7\text{He}$ reaction in inverse kinematics at $29 \text{ A} \cdot \text{MeV}$
 ${}^6\text{He}$ beam delivered by the ACCULINNA-2 fragment separator (FLNR, JINR). The registration

Corresponding author.

of neutrons from ${}^7\text{He} \rightarrow n + {}^6\text{He}$ decay made it possible to derive the ${}^7\text{He}$ ground state parameters, the decay energy of 0.38(2) MeV and width of 0.11(3) MeV.

Keywords: ${}^7\text{He}$ ground state; (dp) reaction.

PACS Number(s): 21.10.Jx, 21.60.Ka, 25.60.Je, 27.20.+n

1. Introduction

The neutron-rich ${}^7\text{He}$ helium isotope was observed for the first time in the ${}^7\text{Li}(t, {}^3\text{He}){}^7\text{He}$ charge exchange reaction more than 40 years ago.¹ The study showed that this nucleus has no nucleon-stable states and its ground state, with a width of 0.17 ± 0.04 MeV, is located 0.42 ± 0.06 MeV above the neutron decay threshold. Since then, numerous studies have been dedicated to investigating this nucleus. While the ground state of ${}^7\text{He}$ has been observed in nearly all of these studies, the resonance parameters varied significantly across different works. Two main experimental techniques can be distinguished here: (i) measuring the spectra of the missing mass (MM) from charge exchange^{1,2} and nucleon exchange reactions^{3–8} or (ii) measuring the spectra of the invariant mass from the fragmentation or knockout reactions.^{9–12} As a rule, experiments related to the measurement of the invariant mass are characterized by greater statistics and better resolution compared to the experiments where the MM spectrum is measured with the use of transfer reaction. However, the analysis of the invariant-mass spectra from different experiments leads to different values of the resonance parameters. For example, in Ref. 9, where the relative energy of ${}^6\text{He}$ and neutron was measured as a result of fragmentation of the ${}^8\text{He}$ beam on a carbon target, the authors came to the assumption that the measured energy spectrum contains, in addition to the ground state ${}^7\text{He}$ ($J^\pi = 3/2^-$), a low-lying spin partner ($J^\pi = 1/2^-$) at an energy of ~ 1.0 MeV above the neutron decay threshold. The energy and width of the ground state were determined as $E_r = 0.43(2)$ MeV and $\Gamma = 0.15(8)$ MeV, respectively. An almost identical experiment performed by the same group of authors¹⁰ but using a liquid hydrogen target did not confirm the presence of the low-lying excited state in ${}^7\text{He}$ and led to the altered values of the ground state parameters, $E_r = 0.387(2)$ MeV and $\Gamma = 0.190(6)$ MeV. The difference clearly extends beyond the statistical error. The paper “Recoil proton tagged knockout reaction for ${}^8\text{He}$ ”¹² presents data from an experiment on the interaction of a ${}^8\text{He}$ beam with an energy of 82.3 MeV/nucleon with a hydrogen target. In order to separate the process of knocking out a valence neutron from the incident ${}^8\text{He}$ beam, the spectrum of the invariant mass (${}^6\text{He} + n$) was measured in coincidences with recoil protons. It appeared that the inclusive invariant-mass spectrum differs significantly from the spectrum measured without coincidence with the recoil protons. The resonance parameters of the ${}^7\text{He}$ ground state obtained from the analysis of the inclusive (measured in coincidence) spectrum were $E_r = 0.38$ (0.43) MeV and $\Gamma = 0.195$ (0.182) MeV, respectively. All this indicates that in the observed fragmentation or knockout reactions, the spectra, carrying information about the resonance parameters, are significantly affected by the reaction mechanism. Hence, to obtain reliable information about the nuclear resonance

states, one should have a detailed knowledge about the mechanism of the reaction populating these states. The most reliable, practically model-free information about the nuclear structure in the continuum-spectrum region can be obtained from a phase analysis of the elastic-scattering excitation function based on the R -matrix theory. It is clear that in the case of ${}^7\text{He}$, it is impossible to experimentally measure the excitation function of the neutron elastic scattering on the ${}^6\text{He}$ nucleus, but the closest process may be the deuteron stripping reaction ${}^6\text{He}(d,p){}^7\text{He}$. Experimental data and numerous DWBA calculations indicate that in the energy region above the Coulomb barrier, the main mechanism of deuteron disruption is the direct neutron transfer, which corresponds to the pole diagram in terms of the dispersion theory.¹³ In Ref. 14 a model was proposed, according to which, in the plane-wave approximation, the partial cross-section of the (d,p) reaction was related to the total cross-section for the interaction of the neutron with the target nucleus.

By now, only two experimental works^{6,15} used the (d,p) reaction to study the structure of ${}^7\text{He}$, and, in the best case, the experimental resolution in the measured excitation energy spectrum was ~ 350 keV, i.e., it noticeably exceeds the value of ${}^7\text{He}$ width $\Gamma_{\text{res}} = 0.132$ MeV predicted by the recent ab-initio no-core calculations shown in Table 2 of Ref. 16. The aim of this work is to measure the ${}^6\text{He}(d,p){}^7\text{He}$ reaction products in inverse kinematics with a beam of ${}^6\text{He}$ nuclei with full kinematic reconstruction. Not only protons from the transfer reaction were detected in the experiment but also all decay products ${}^7\text{He} \rightarrow {}^6\text{He} + n$, whereas the main part of the decay energy was carried away by the neutron, which made it possible to significantly improve the experimental resolution of the experiment by the time-of-flight (ToF) measurement of the neutron energy.

2. Experiment

The experiment was performed in 2020 at the ACCULINNA-2 radioactive-ion beam separator installed at the U-400M heavy-ion cyclotron, Flerov Laboratory of Nuclear Reaction (JINR, Dubna).¹⁷ The secondary ${}^6\text{He}$ beam with an intensity of 8×10^5 1/s and energy $29 \text{ A} \cdot \text{MeV}$ was produced via the fragmentation of the primary ${}^{11}\text{B}$ beam nuclei accelerated by the U-400M cyclotron to $33.4 \text{ A} \cdot \text{MeV}$. The experimental setup is shown in Fig. 1. The ${}^6\text{He}$ beam bombarded a target filled with deuterium gas at temperature 26 K and pressure 1.48 atm . The 6 mm-thick and 25 mm-diameter target cell was hermetically sealed with two $6\text{ }\mu\text{m}$ thick stainless-steel windows. This provided the target thickness 3.4×10^{20} atoms/cm².

The ${}^6\text{He}$ beam energy was measured using a standard time-of-flight (ToF) technique with two detectors based on the fast plastic scintillators (EJ-212) with a thickness of $125\text{ }\mu\text{m}$ each (see the ToF_F3 and ToF_F5 detectors in Fig. 1). The detectors were installed at a distance of 12.35 m from each other allowing for the particle identification and ToF measurement, made for the ${}^6\text{He}$ beam nuclei with uncertainty of 0.5 ns. Two multi-wire proportional chambers (MWPC), installed upstream the target at a distance of 270 and 814 mm, were used to determine the

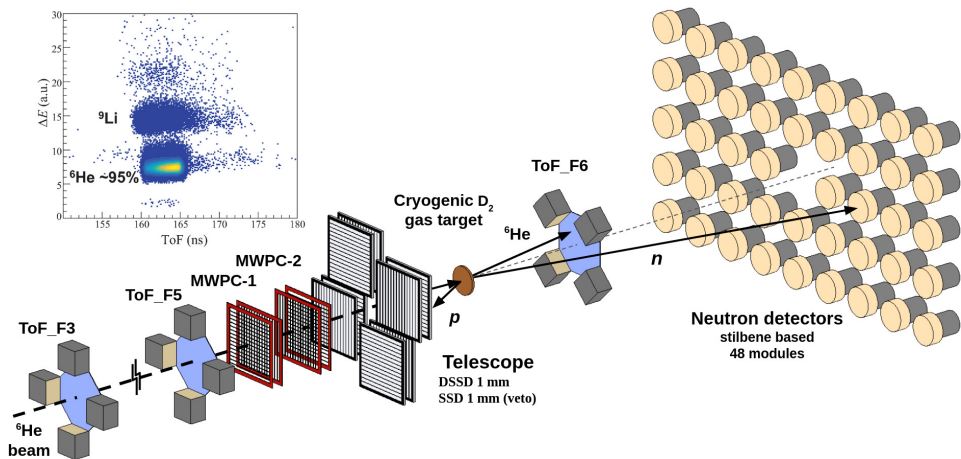


Fig. 1. Experimental setup used in the study of the $^2\text{H}(^6\text{He}, p)^7\text{He}$ reaction with the ^6He secondary beam at the ACCULINNA-2 fragment separator. The time-of-flight scintillation sensors (ToF_F3, F5), position-sensitive beam detectors (MWPC-1, 2) and array of four detector telescopes based on square silicon detectors are installed upstream of the D_2 cryogenic gas target. Behind the target were installed a plastic scintillator (ToF_F6) and an array of neutron detectors. See text for the details.

trajectories of the incident ^6He nuclei and their coordinates on the target plane. As a result, the interaction point was determined with an accuracy better than 1.5 mm.

The energy and the emission angles of the flying backward proton recoils were measured with an array of four detector telescopes located upstream at a distance of 134 mm from the target (see designation Telescope in Fig. 1). Being compactly placed along a plane with a shift relative to each other, the telescopes detected the reaction product emitted from the target in the angular range of $\sim 150\text{--}170^\circ$ relative to the beam direction in the laboratory system and, moreover, the free beam passage to the target was provided. Each telescope consisted of two square silicon detectors, $64 \times 64 \text{ mm}^2$ in size and 1 mm thick. The double-sided detectors (DSDs), mounted in front, closer to the target, had 32×32 strips and provided the measurement of the energy and the detection positions of the protons emitted from the target. The next, single-sided detectors (SSDs) were used for the veto signals. The detectors were calibrated with α -particles emitted from the ^{226}Ra source.

The plastic scintillator (EJ-212), 100 mm in diameter and 250 μm thick, was installed on the beam axis 83 cm downstream the target. This detector (see the ToF_F6 in Fig. 1) is hereinafter referred to as F6.

The registration of neutrons was performed using an array of detectors with 48 modules based on stilbene crystals¹⁸ with a low ($< 100 \text{ keV}$) threshold for $n - \gamma$ discrimination. The detector array was installed behind the reaction chamber at a distance of 3 m from the target. In this case, the outlet window of the reaction chamber was made of stainless steel with a wall thickness of 180 μm . The neutron energy was measured by the ToF method. Observation of the γ -peak with 0.6 ns (FWHM) from the interaction of the beam with target provides the absolute

calibration and the accuracy of neutron energy measurements. The time resolution for 3 m ToF base corresponds to 500 keV energy resolution (FWHM) for registration of neutron with 20 MeV energy. It might be considered as the upper limit of energy resolution because the time resolution depends on the amplitude of the detector response which is larger for neutron hits with the energy of interest in comparison with gammas.

In the experiment, two triggers were used to start data acquisition system. The main trigger was taken from any of the DSDs. The other one was taken from the plastic scintillators F5 (see the ToF_F5 in Fig. 1) with the 4096-fold count-rate reduction and was used for beam intensity monitoring.

3. MM Spectrum

Figure 2 shows the two-dimensional distribution obtained for the events corresponding to the coincidence registration of the recoil protons from the reaction ${}^2\text{H}({}^6\text{He}, p){}^7\text{He}$ with the charged products of the ${}^7\text{He} \rightarrow {}^6\text{He}(0^+) + n$ or ${}^7\text{He} \rightarrow {}^6\text{He}(2^+) + n \rightarrow \alpha + 3n$ decay recorded by the F6 detector. The horizontal axis in Fig. 2 shows the ${}^7\text{He}$ decay energy E_{cm} above the ${}^7\text{He} \rightarrow {}^6\text{He} + n$ threshold. The vertical axis shows the F6 time, which is the difference between the measured ToF of the ${}^7\text{He}$ charged decay particles (${}^6\text{He}$ or α) and the calculated ToF of the beam ions. This quantity depends on the detected particle longitudinal momentum. The trapezoidal area marked in Fig. 2 with the solid line confines the range of ToF values for the events from the ${}^7\text{He}$ decay and clearly demonstrates an increase in the longitudinal momentum range appearing with the increase of the ${}^7\text{He}$ excitation energy. Events lying outside this structure correspond to the background generated mainly by the random coincidences of protons with the products of the beam interaction with the material of the target windows.

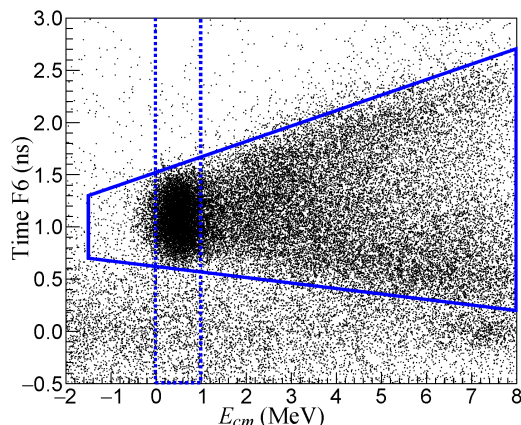


Fig. 2. Decay energy E_{cm} (or MM spectrum) of ${}^7\text{He}$ from the ${}^2\text{H}({}^6\text{He}, p)$ reaction versus time-of-flight ToF of the charged decay products of ${}^7\text{He}$ measured between the target and the F6 detector. The spectrum was obtained by registration of the recoil proton in coincidence with ${}^4\text{He}$ or ${}^6\text{He}$ from ${}^7\text{He}$ decay.

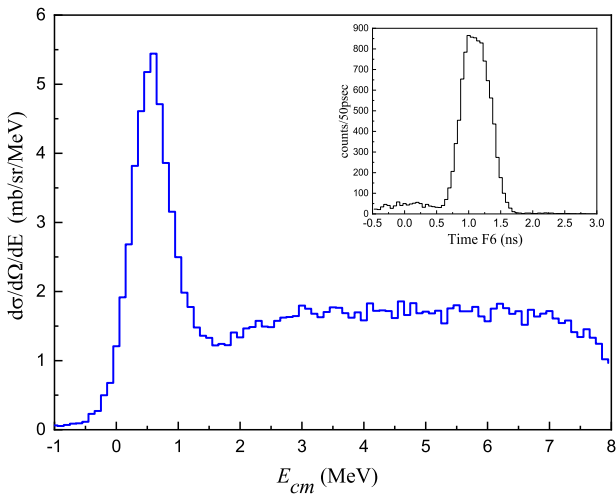


Fig. 3. Experimental MM spectrum of ${}^7\text{He}$ obtained for events limited by the trapezoidal contour shown in Fig. 2. Inset shows the projection of the region of the ground-state peak (0–1 MeV) on the Time F6 axis in Fig. 2.

The MM spectrum of ${}^7\text{He}$ corresponding to the events taken within the selected trapezoidal region of the two-dimensional plot (see in Fig. 2) is shown in Fig. 3. The spectrum is dominated by the peak corresponding to the population of the ${}^7\text{He}$ nucleus in its ground state ($J^\pi = 3/2^-$). The peak full width at half of maximum (FWHM) of ~ 600 keV noticeably exceeds the intrinsic ${}^7\text{He}$ ground-state width and demonstrates the experimental resolution, which is mainly determined by the target thickness and energy losses of the detected protons having relatively low energy (2–5 MeV). Inset in Fig. 3 shows the projection of the events corresponding to the population of the ${}^7\text{He}$ ground state (rectangular area shown by the dotted lines in Fig. 2). It demonstrates that the background does not exceed a few-percent part of the total number of counts obtained in the region of the ground-state peak.

4. DWBA Calculations

The recoil protons were detected in the range of ~ 150 – 170° in the laboratory frame, which corresponds to ~ 5 – 10° in the center-mass system of the ${}^2\text{H}({}^6\text{He}, p){}^7\text{He}_{\text{g.s.}}$ reaction. The angular distribution measured for this reaction is shown at Fig. 4 by the black filled circles, together with the similar data from Ref. 6 measured at $E_{\text{lab}} = 11.5$ MeV/u (open circles). The error bars are statistical, with an estimated uncertainty of the absolute normalisation as 10% mainly due to the uncertainty introduced by the target thickness. Differential cross-sections were calculated within the DWBA method. This requires knowledge of the nucleus–nucleus optical potential (OPs) parameters for the entrance and exit channels. It is difficult to obtain this due to the lack of relevant data on the elastic scattering cross-sections. However, in Ref. 19 the cross-section of the transfer reaction ${}^6\text{Li}(d, {}^7\text{Li})p$ was measured at the

Properties of the ${}^7\text{He}$ ground state studied by the ${}^6\text{He}(d,p){}^7\text{He}$ reaction

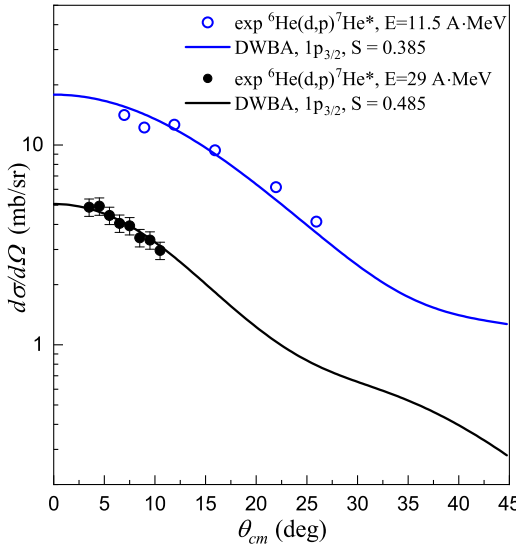


Fig. 4. Angular distributions for the ${}^2\text{H}({}^6\text{He}, p){}^7\text{He}_{\text{g.s.}}$ reaction measured at $E_{\text{lab}} = 11.5 \text{ MeV/u}$ (open circles,^a) and 29 MeV/u (solid circles, this work). The curves represent the DWBA calculations described in the text.

deuteron projectile energy 50 MeV. These results were analyzed within the framework of the channel coupling method and the parameterization of the optical potentials in the entrance $d + {}^6\text{Li}$ and exit $p + {}^7\text{Li}$ channels was proposed. Using the OPs found in Ref. 19, we refined the values of the parameters for an adequate description of the elastic scattering data within the optical model. The values thus obtained, characterizing the OPs, are given in Table 1. The optical potentials are determined in the classical form, as the sum of the Coulomb and complex nuclear components. Note that the parameters presented in Table 1 differ from the OPs reported in Ref. 19 only by the increased diffuseness value a_V for the $d + {}^6\text{Li}$ potential.

The ${}^6\text{Li}$ optical parameters in Table 1 were used to calculate the transfer cross-section for the reaction of interest, assuming the similarity of these reactions. The

Table 1. Optical model potential.

$\mathcal{R}e$ form-factor	V_0 , MeV	r_v^a , fm	a_v , fm	$\mathcal{I}m$ form-factor	W_0 , MeV	r_w , fm	a_w , fm	r_C , fm
n + p	Gaussian	52.92	1.800					
n + ${}^6\text{He}$	WS(vol)	44.54	1.250	0.650				
d + ${}^6\text{Li}$	WS(vol)	81.30	1.137	0.790	WS(surf)	10.80	1.128	0.738
p + ${}^7\text{Li}$ ^b	WS(vol)	55.00	1.069	0.674	WS(vol)	8.86	1.730	1.240
								1.30

Notes: ^aRadii of optical potentials are defined in the form $R_i = r_i A_{\text{targ}}^{1/3}$, where A_{targ} is the mass number of the heaviest reaction participant.

^bThis OP also includes the spin-orbit interaction of the Thomas form with parameters: $V_{SO} = 4.9 \text{ MeV}$, $r_{SO} = 1.0 \text{ fm}$, $a_{SO} = 0.53 \text{ fm}$.

cross-sections were calculated using the DWUCK5 code²⁰ integrated into the NRV knowledge base.²¹ To calculate the wave functions of the bound states, we used the standard method of adjusting the potential-well depth to reproduce the neutron binding energy at the given quantum numbers. The deuteron was considered as the $1s$ state of the $p + n$ system with the binding energy $\varepsilon_d = 2.225$ MeV. The corresponding potential parameters are given in Table 1. In the final state, the neutron is unbound. The resonance state of ${}^7\text{He}$ was treated as “almost bound”, supposing the weak binding of the $n + {}^6\text{He}$ system $\varepsilon_{{}^7\text{He}} = -0.1$ MeV but retaining the correct Q -value. The potential providing the $1p3/2$ state wave function for the $n + {}^6\text{He}$ system is also presented in Table 1.

The DWBA cross-sections calculated in accordance with the above scheme are presented by curves in Fig. 4 that demonstrate quantitative agreement with the measured data. To fit the experimental data, the DWBA calculations were normalized with the spectroscopic factors. The presented curves correspond to the spectroscopic factors 0.49 for our measurements and 0.39 for the data at $E_{\text{lab}} = 11.5$ MeV/u.⁶ A value of 0.49 coincides well with the theoretical estimations,²² whereas the results of Ref. 6 lead to a $\sim 30\%$ lower value.

5. Coincidences with Neutrons

Coincidences with neutrons from the decay of ${}^7\text{He}$ were also detected in the present experiment. The neutron detector covers the angles up to 20° in the laboratory system, which corresponds to the maximal neutron emission angles in the decay of ${}^7\text{He}$ with excitation energy up to 1.5 MeV. At higher excitation energies, the neutron emission cone in the laboratory system exceeds the angular acceptance of the

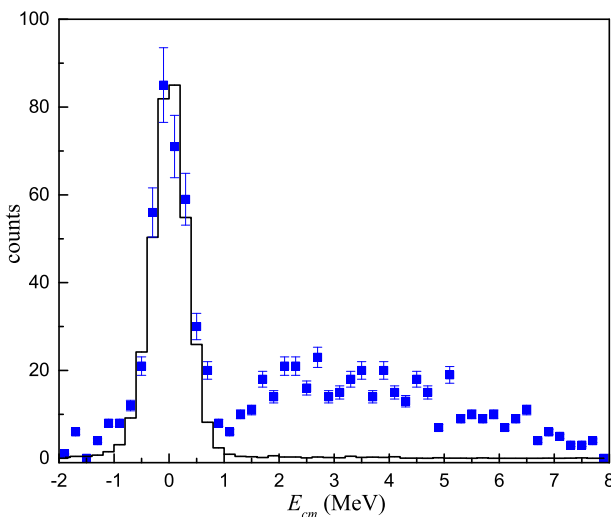


Fig. 5. ${}^6\text{He}$ MM spectrum from the reaction ${}^2\text{H}({}^6\text{He}, pn){}^6\text{He}$ reconstructed from the proton–neutron coincidence events. The histogram shows the result of MC simulation for the ${}^2\text{H}({}^6\text{He}, p){}^7\text{He}_{\text{g.s.}}$ reaction.

detector, and the detection efficiency of coincidences with neutrons drops sharply. However, even in the region of full angular acceptance, the neutron detection efficiency is at the level of several percent. Nevertheless, the registration of neutrons (which corresponds to the conditions of a complete kinematic experiment) makes it possible to significantly improve the instrumental resolution. Figure 5 shows the MM spectrum of ^6He reconstructed from the $^7\text{He} \rightarrow ^6\text{He} + n$ decay by taking the proton-neutron coincidence events. The experimental data are presented as dots with error bars. The histogram shows the result of Monte-Carlo (MC) simulation, which takes into account the details of the experimental setup, using the GEANT4 software package. Zero of the scale corresponds to the ^6He formation in its ground state. The continuous spectrum above the $^6\text{He}^* \rightarrow \alpha + 2n$ threshold conforms the proton coincidences with the neutrons from both the $^7\text{He} \rightarrow ^6\text{He} + n$ and (mostly) from the $^6\text{He}^* \rightarrow \alpha + 2n$ decay.

Figure 6 shows the excitation energy spectrum of ^7He for the events where the coincidences of the protons and neutrons from the reaction $^2\text{H}(^6\text{He},p)^7\text{He} \rightarrow ^6\text{He}_{\text{gs}} + n$ were fixed. The experimental data are shown as points with statistical errors, the solid line is the MC calculation where the ^7He ground-state decay energy distribution was parameterized as a Breit-Wigner line shape with an energy-dependent width and the values of R -matrix parameters $E_{\text{res}} = 0.38\text{ MeV}$ and $\Gamma_{\text{res}} = 0.11\text{ MeV}$. The instrumental resolution was estimated to be $\sim 140\text{ keV}$ (FWHM), a value comparable

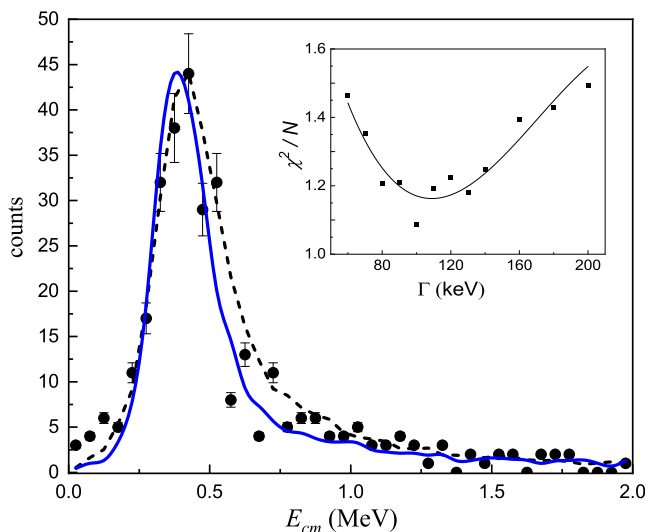


Fig. 6. The ^7He excitation energy spectrum obtained for the reaction channel $^2\text{H}(^6\text{He},p)^7\text{He} \rightarrow ^6\text{He}(\text{g.s.}) + n$. The spectrum is reconstructed from the proton-neutron coincidence events (filled circles with error bar). The solid line is the result of MC calculations with R matrix parameters $E_{\text{res}} = 0.38\text{ MeV}$ and $\Gamma_{\text{res}} = 0.11\text{ MeV}$ for the ^7He ground-state resonance. The inset shows the dependence of χ^2/N on the resonance width. For illustration, the dashed line shows a simulation curve with the assumed ^7He parameters that are taken from the NUDAT database. ($E_{\text{res}} = 0.41\text{ MeV}$ and $\Gamma_{\text{res}} = 0.15\text{ MeV}$, <https://www.nndc.bnl.gov/nudat3/>).

A. A. Bezbakh *et al.*

to the resonance intrinsic width. The inset shows the dependence of χ^2/N value on the resonance width calculated for the energy range from 0.2 to 0.95 MeV.

6. Summary

The excitation energy spectrum of ${}^7\text{He}$ was measured in the range of 0–7 MeV in the reaction ${}^2\text{H}({}^6\text{He}, p)$. The peak corresponding to the formation of ${}^7\text{He}$ in the ground state ($J^\pi = 3/2^-$) dominates in the lower part of the spectrum. The angular distribution for ${}^7\text{He}_{\text{g.s.}}$ was measured in the range of $\sim 5\text{--}10^\circ$ in the center of mass system of the (d, p) reaction and is well reproduced by the DWBA calculation with the spectroscopic factor $S = 0.485$. This value is $\sim 30\%$ larger than that obtained in the previous measurement of the same reaction at a beam energy of 11.5 MeV/u,⁶ but close to the value of 0.53 resulting from the calculation of the type described in Ref. 22. The detection of decay neutrons in coincidence with recoil protons provided kinematically complete measurements which allowed for fine resolution in the derived excitation spectrum of ${}^7\text{He}$, comparable to the intrinsic width of the ${}^7\text{He}$ ground state. As a result, our estimation of the ${}^7\text{He}$ ground state resonance parameters $E_{\text{res}} = 0.38(2)$ MeV and $\Gamma = 0.11(3)$ MeV. The obtained width is appreciably smaller in comparison with the previous results ($\Gamma = 0.182(5)$ ¹² or $\Gamma = 0.14$ MeV²³). It should be noted for future experiments that the method of detection of decay neutrons allows for much better instrumental resolution in comparison with detection of charged fragments, which in turn reduces impact of the setup details on the intrinsic width evaluation.

Acknowledgments

This work was partly supported by the Russian Science Foundation grant No. 22-12-00054 and by NCPhM, theme No. 6 “Nuclear and radiation physics”. The authors appreciate the L. V. Grigorenko, E. Yu. Nikolskii and P. G. Sharov valuable and useful comments. We acknowledge the interest and support of this activity from Profs. Yu. Ts. Oganessian and S. N. Dmitriev.

ORCID

- A. A. Bezbakh  <https://orcid.org/0000-0002-5280-8699>
- M. S. Golovkov  <https://orcid.org/0009-0002-2988-2820>
- A. S. Denikin  <https://orcid.org/0000-0002-1913-3693>
- R. Wolski  <https://orcid.org/0000-0003-2653-2112>
- S. G. Belogurov  <https://orcid.org/0000-0002-6879-2767>
- V. Chudoba  <https://orcid.org/0000-0002-0419-2025>
- E. M. Gazeeva  <https://orcid.org/0000-0002-6415-3052>
- A. V. Gorshkov  <https://orcid.org/0000-0003-3011-9670>
- G. Kaminski  <https://orcid.org/0000-0001-5628-1276>

- B. R. Khamidullin  <https://orcid.org/0009-0000-9163-628X>
M. Khirk  <https://orcid.org/0000-0002-0494-1938>
S. A. Krupko  <https://orcid.org/0000-0003-3227-9643>
B. Mauyey  <https://orcid.org/0000-0003-4301-1327>
A. M. Quynh  <https://orcid.org/0000-0002-0044-3464>
A. Swiercz  <https://orcid.org/0000-0001-7911-3849>
G. M. Ter-Akopian  <https://orcid.org/0000-0003-0485-6650>

References

1. R. H. Stokes and P. G. Young, *Phys. Rev. Lett.* **18** (1967) 611.
2. R. H. Stokes and P. G. Young, *Phys. Rev.* **178** (1969) 2024.
3. A. A. Korsheninnikov *et al.*, *Phys. Rev. Lett.* **82** (1999) 3581.
4. H. G. Bohnen *et al.*, *Phys. Rev. C* **64** (2001) 024312.
5. F. Skaza *et al.*, *Phys. Rev. C* **73** (2006) 044301.
6. A. H. Wuosmaa *et al.*, *Phys. Rev. C* **72** (2005) 061301.
7. A. H. Wuosmaa *et al.*, *Phys. Rev. C* **78** (2008) 041302.
8. F. Renzi *et al.*, *Phys. Rev. C* **94** (2016) 024619.
9. M. Meister *et al.*, *Phys. Rev. Lett.* **88** (2002) 102501.
10. Y. Aksyutina *et al.*, *Phys. Lett. B* **679** (2009) 191.
11. D. H. Denby *et al.*, *Phys. Rev. C* **78** (2008) 044303.
12. Z. X. Cao *et al.*, *Phys. Lett. B* **707** (2012) 46.
13. I. S. Shapiro, *Selected Topics in Nuclear Theory* (I.A.E.A., Vienna, 1963).
14. R. Lipperheide, *Phys. Lett. B* **32** (1970) 555.
15. M. S. Golovkov *et al.*, *Phys. At. Nucl.* **64** (2001) 1244.
16. I. A. Mazur *et al.*, *Phys. Rev. C* **106** (2022) 064320.
17. A. Fomichev *et al.*, *Eur. Phys. J. A* **54** (2018) 97.
18. A. Bezbakh *et al.*, *Instrum. Exp. Tech.* **61** (2018) 631.
19. A. T. Rudchik *et al.*, *Nucl. Phys. A* **602** (1996) 211.
20. P. Kunz, DWUCK5: Distorted wave Born approximation — Computer code (1992), <https://www.oecd-nea.org/tools/abstract/detail/nesc9872>.
21. A. V. Karpov *et al.*, *Nucl. Instrum. Methods Phys. Res. A* **859** (2017) 112.
22. S. C. Pieper *et al.*, *Phys. Rev. C* **70** (2004) 054325.
23. S. Huang *et al.*, *Few-Body Syst.* **62** (2021) 102.